JOURNAL OF MATERIALS SCIENCE 33 (1998) 5849–5853

Correlation of grain-boundary precipitates parameters with fracture toughness in an Al–Cu–Mg–Ag alloy subjected to long-term thermal exposure

B. Q. Li
McCook Metals L.L.C, 4900 First Avenue, McCook, IL 60525, USA
E-mail: bqli@lanmail.rmc.com

A. P. REYNOLDS
University of South Carolina, Department of Mechanical Engineering, Columbia, SC 29208, USA

The effect of thermal exposure on grain-boundary precipitation in Al–Cu–Mg–Ag alloy was studied using quantitative transmission electron microscopy. Grain-boundary precipitate parameters, such as average size, number density and precipitate-free zone width, were measured. The effective diameter of precipitates, number of precipitates per grain-boundary area and area fraction of precipitates on the grain boundary were calculated. These data were applied to a grain-boundary fracture model to calculate grain-boundary fracture strain. The calculated fracture strains, in turn, were used to check the validity of two existing models of fracture toughness, which are based on grain-boundary nucleation of cracks and their propagation through precipitate-free zones. The fracture toughness model of Hornbogen and Graf closely agrees with the experimental results.

1. Introduction

Al–Cu–Mg–Ag alloys, strengthened by the Ω phase, have been of interest recently in the aerospace and aeronautic industry because of their excellent thermal stability [1]. The alloys have been considered as candidate materials for potential elevated temperature applications. Although the alloys retain their favourable tensile properties after exposure to temperatures below 120 °C, they undergo fracture toughness degradation after a long-term thermal exposure at higher temperature [2]. Study has shown that at 135 °C long duration thermal exposure, these alloys suffer both yield strength and fracture toughness degradation [2]. Recent studies have shown that area fraction of ductile intergranular fracture increases with increase in thermal exposure temperature and times, and that precipitates coarsen significantly in the matrix at 135 °C in these Al–Cu–Mg–Ag alloys [3, 4].

Correlation between the mechanical properties and microstructural parameters has long been pursued by metallurgists. Several models have been developed which describe the relationship between fracture toughness and grain-boundary microstructural characteristics [5]. These models predict an increase in yield strength with a decrease in fracture toughness. However, there are very few experimental attempts to link grain-boundary microstructural parameters with bulk aluminium alloy fracture properties. The objective of the present study was to investigate the effect of long-term elevated temperature exposures on the microstructural parameters of the grain boundary, and to correlate these parameters to fracture toughness of an Al–Cu–Mg–Ag alloy.

2. Experimental procedure

The test alloy was obtained from ALCOA in the form of a 2.3 mm thick sheet and has a nominal composition (wt %) of 5.4Cu–0.5Mg–0.5Ag–0.12Zr–0.3Mn, balance Al. The thermo-mechanical processing in the production of the sheet, combined with the presence of numerous large constituent particles led to a recrystallized microstructure with a near random texture [6]. The alloy was heat treated to a commercial T8 condition and exposed at 135 °C for 1000 and 3000 h.

Grain-boundary characterization of the alloy was performed using transmission electron microscopy (TEM). A Philips EM 420 equipped with EDS and a double tilt holder was used for the analysis. TEM specimens were cut from the alloy, then electrolytically polished at −30°C and 12 V in a 30% HNO_3 + 70% methanol bath. The thin region of TEM foil was near the t/2 location in the sheet. Because the texture was weak, grain boundaries were selected randomly. A

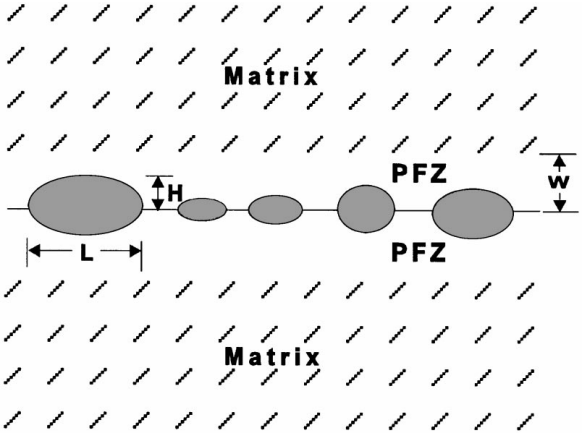

Figure 1 Schematic illustration of grain-boundary and precipitate parameters.

grain boundary was tilted to the edge-on position, and a TEM image was taken near the thin foil edge in order to avoid overlap of grain-boundary precipitates. The foil thickness in the area of interest is of the order of the precipitate diameter. This avoids the need for foil thickness measurements and allows treatment of the data as a two-dimensional problem. More than 20 TEM negatives (all at a magnification of $\times 68000$) with different grain boundaries were taken for analysis at each exposure condition. The grain-boundary features were measured using a low-power magnifier ($\times 10$) and a scale with a resolution of 0.1 mm. The parameters extracted from such measurements included: precipitate line density at the grain boundary, n_1, or number of precipitates per length of grain boundary; width of precipitate free zone, W; precipitate size: length, L, and thickness, H, as shown in Fig. 1. These parameters can be further manipulated to obtain the number of precipitates per unit area of grain boundary, $N_s = n_1^2$; mean size of grain boundary precipitates, $D = (LH)^{1/2}$, and area fraction of grain-boundary precipitates, $A_f = \pi(D/2)^2 N_s$. Here the relationship of $D = (LH)^{1/2}$, the mean size of precipitate, is based on the observation that the grain-boundary precipitates are more oval shaped than spherical: the dimensions of the precipitates in the plane of the boundary are, in general, better represented by the relationship shown than by the use of L alone. Because of the narrow distribution of grain-boundary particle sizes, we also made the approximation that $\langle r \rangle^2 \approx \langle r^2 \rangle$.

Room-temperature tensile properties of the alloy were measured in three conditions, namely, T8, T8 + exposed for 1000 h/135 °C and T8 + exposed for 3000 h/135 °C. As the test alloy was obtained in sheet product form, a measure of the crack growth toughness was desired. Hence, the following procedure was used to provide a measure of the resistance to crack growth: L–T orientation compact tension specimens with $W =$ 50.8 mm were machined from the sheet; the specimens were tested in accordance with ASTM E1152–87, "Standard Test Method for Determining J–R Curves"; the single specimen method with determination of crack length via unloading compliance was used. The reported toughness is that corresponding to $(JE)^{1/2}$ at a crack extension of 2 mm, where J is the value of the applied J-integral at $\Delta a = 2$ mm and E is Young's modulus of the alloy.

3. Results

The primary strengthening precipitate in the T8 condition of the alloy is the Ω phase which forms on {1 1 1} matrix planes, and with chemical composition Al_2Cu [7, 8]. The other precipitates coexisting with the Ω phase in the alloys are S′ and θ' phases. Fig. 2 shows the Ω phase in the matrix of the alloy in the T8 condition (electron beam parallel to $\langle 0\,1\,1 \rangle_{Al}$). Two variants of the Ω phase can be seen in edge-on orientation. The grain-boundary precipitates were determined as the Ω phase. Grain-boundary precipitates were larger than those in the matrix. Their morphology appeared dependent on the plane of the grain boundary. High-resolution TEM observation indicates that the grain-boundary Ω phase is likely to form on the {1 1 1} facets of the grain-boundary plane, and that its morphology is that of a thick plate. At relatively low magnification ($< \times 10^5$) and with geometry restrictions (grain-boundary plane must be parallel to the electron beam), however, the grain-boundary precipitates can be treated as allotriomorphic and the grain boundary as a straight line. In Fig. 3 the grain-boundary precipitates are shown for the T8 and T8 + 135 ° C/3000 h conditions. Grain-boundary parameters of the alloy with three different thermal exposure conditions are listed in Table I.

In Fig. 4, the alloy yield strength as a function of exposure time is shown for a 135 °C exposure temperature. Reduction of the yield strength following thermal

TABLE I Grain-boundary parameters

T. E. condition	W (μm)	D (μm)	N_s (μm^{-2})	A_f
T8	0.028	0.013	3387	0.464
T8 + 135 °C/10^3 h	0.033	0.020	2224	0.706
T8 + 135 °C/3 × 10^3 h	0.040	0.023	1939	0.799

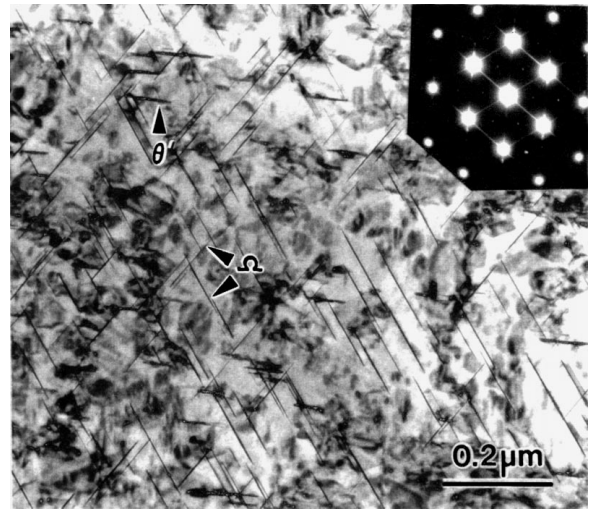

Figure 2 Ω precipitates along $\langle 0\,1\,1 \rangle_{Al}$ direction, with two variants of the Ω phase in the matrix. The SAD pattern (insert) shows the streaks along the $\langle 1\,1\,1 \rangle$ direction.

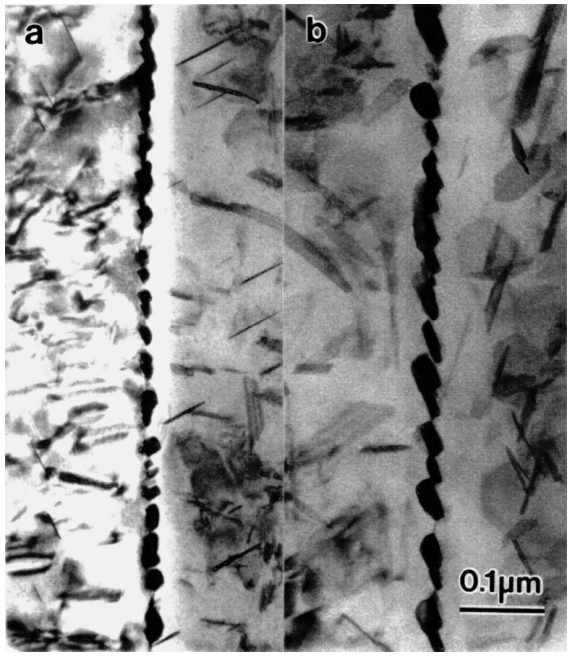

Figure 3 (a) Grain boundary in the T8 condition, and (b) after 3000 h exposure at 135 °C.

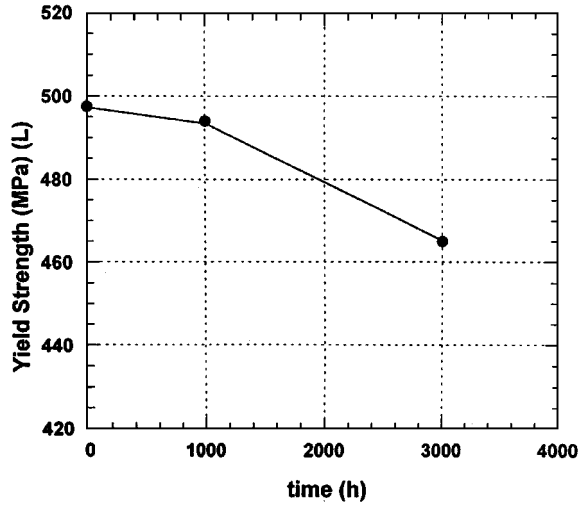

Figure 4 Tensile yield strength as a function of exposure time at 135 °C.

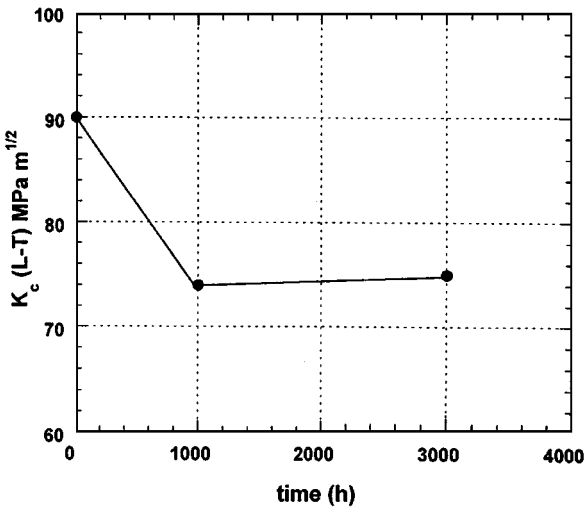

Figure 5 Fracture toughness as a function of exposure time at 135 °C.

exposure at 1000 and 3000 h indicates that coarsening of the matrix Ω has occurred in the alloy [4]. The effect of exposure on fracture toughness, determined at crack extension $\Delta a = 2$ mm, is shown in Fig. 5. A drop in fracture toughness for the 1000 h exposure with respect to the T8 condition can be seen. Between 1000 and 3000 h exposure, fracture toughness value increases slightly. Fractography indicates that intergranular fracture with shallow dimples, becomes more prevalent after long-term thermal exposures [3]. Reynolds and co-workers observed that area fraction of the intergranular fracture increases dramatically as a function of exposure time at 135 °C [2, 3].

4. Discussion

To correlate the microstructural parameters of grain-boundary precipitates with mechanical properties at the grain boundary, an equation developed by Kawabata and Izumi [9] was applied. Kawabata and Izumi [9] developed a model to calculate fracture strain at grain boundaries, which is based on microstructural parameters of the grain boundary. The model treats the ductile intergranular fracture as a function of characteristic grain-boundary parameters, such as precipitate size, precipitate-free zone (PFZ) width, and number of grain-boundary precipitates per unit grain-boundary area. Based on the idea that fracture occurs due to void formation at interfaces between the grain-boundary precipitates and the matrix, and that their growth and coalescence occurs in the PFZs, they derived an equation to describe the fracture strain. The fracture strain, $\varepsilon_{\mathrm{fi}}$, at the grain boundary is expressed approximately as

$$\varepsilon_{\mathrm{fi}} = k\frac{W}{D^3 N_{\mathrm{s}}} \tag{1}$$

where k is a constant related to interfacial energy between grain-boundary precipitate and the matrix, and strain ratio of the PFZ to the grain interior [9], W is the PFZ width, D is the size of grain-boundary precipitate, and N_{s} is the number of grain-boundary precipitates per unit area. Using the parameters from Table I, $\varepsilon_{\mathrm{fi}}$ are calculated and listed in Table II.

Fractographic observations for the three conditions show that the area fraction of intergranular fracture increases after 1000 and 3000 h thermal exposure at 135 °C [2, 3]. This indicates that voids nucleate at the grain boundary, and crack propagation takes place along the soft PFZ region. Based on cracks propagating along the soft cell wall (PFZ), a model was developed by Hornbogen and Graf [10]. To correlate fracture toughness, yield strength and microstructural parameters as

TABLE II Mechanical properties and grain-boundary precipitation parameters as a function of elevated temperature exposure time

T.E. time (h)	K_{c} (MPa m$^{1/2}$)	σ_{y} (MPa)	σ_{yi} (MPa)	$\varepsilon_{\mathrm{fi}} = W/D^3 N_{\mathrm{s}}$ (%)	$(\sigma_{\mathrm{yi}}\varepsilon_{\mathrm{fi}}W)^{1/2}$ ((MPa m)$^{1/2}$)
0	90	498	305	3.61	5.55
1000	74	494	298	1.85	4.26
3000	75	465	285	1.72	4.43

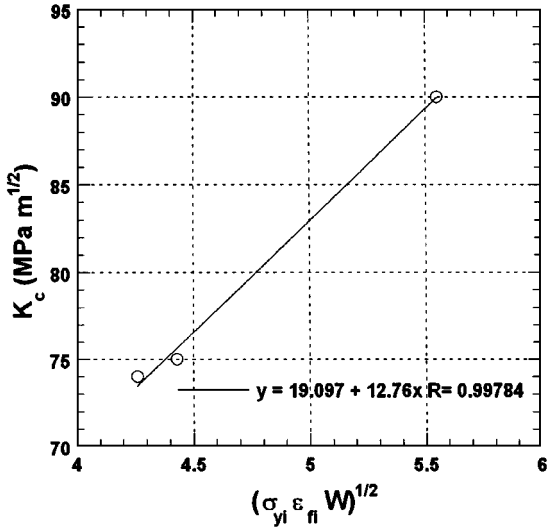

Figure 6 Experimental K_c versus $(\sigma_y \varepsilon_{fi} W)^{1/2}$ for the Hornbogen–Graf model. (——) $y = 19.097 + 12.76x$, $R = 0.99784$.

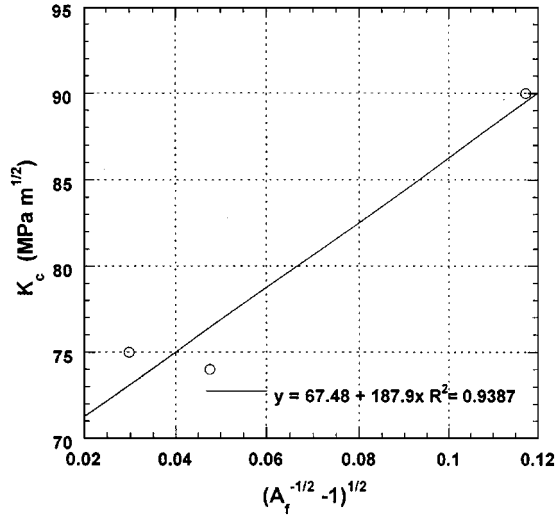

Figure 8 Experimental K_c versus $(A_f^{-0.5} - 1)^{1/2}$ for the Embury–Nes model. (——) $y = 67.48 + 187.9x$, $R^2 = 0.9387$.

given by the following equation

$$K_{lc} = \left(\frac{E \sigma_{yi} \varepsilon_{fi} W}{C S_B} \right)^{1/2} \tag{2}$$

where K_{lc} is the plane strain fracture toughness, E is Young's modulus, σ_{yi} is the yield strength at the grain boundary, ε_{fi} is the fracture strain at the grain boundary, W is the PFZ width, C is a constant, and S_B is the grain size. Because E, C, S_B are constants, and $\varepsilon_{fi} \propto W/D^3 N_s$, the equation can be written as

$$K_{lc} \propto (\sigma_{yi} \varepsilon_{fi} W)^{1/2} \tag{3}$$

In our work, we make the assumption that when the alloy is in the T8 condition, the strength of the PFZ material, σ_{yi}, is equal to the alloy strength in the T4 condition. Then, following Hornbogen and Graf [10], we assume a linear relationship between the overaged alloy strength and the PFZ strength. The calculated values of $(\sigma_{yi} \varepsilon_{fi} W)^{1/2}$, fracture strain, yield strength and fracture toughness as a function of thermal exposure time at 135 °C, are listed in Table II.

Using the data from Table II, the fracture toughness, K_c, was plotted as a function of $(\sigma_y \varepsilon_{fi} W)^{1/2}$ as shown in Fig. 6. The results show a perfect linear relationship. For comparison, the grain-boundary parameters obtained in the present study were used in an alternate model developed by Embury and Nes [11]. Based on their model, K_c is proportional to $(\varepsilon_{fi})^{1/2}$ and also K_c is proportional to $(A_f^{-0.5} - 1)^{1/2}$ [11]. However, Fig. 7, which is a plot of K_c versus $(\varepsilon_{fi})^{1/2}$, and Fig. 8, which is a plot of K_c versus $(A_f^{-0.5} - 1)^{1/2}$ do not show such a good fit as that obtained in Fig. 6. Variation of K_c with the three grain-boundary microstructural parameters, $(\sigma_y \varepsilon_{fi} W)^{1/2}$, $\varepsilon_{fi}^{1/2}$, and $(A_f^{-0.5} - 1)^{1/2}$ plotted against exposure time at 135 °C, is shown in Figs 9–11. As shown in Fig. 9, the trend in the variation of K_c with exposure time is correctly duplicated by the parameter $(\sigma_y \varepsilon_{fi} W)^{1/2}$. Such is not the case for variations of either $\varepsilon_{fi}^{1/2}$ and $(A_f^{-0.5} - 1)^{1/2}$ (see Figs 10 and 11) for the exposure time of 3000 h. Both $\varepsilon_{fi}^{1/2}$ and $(A_f^{-0.5} - 1)^{1/2}$

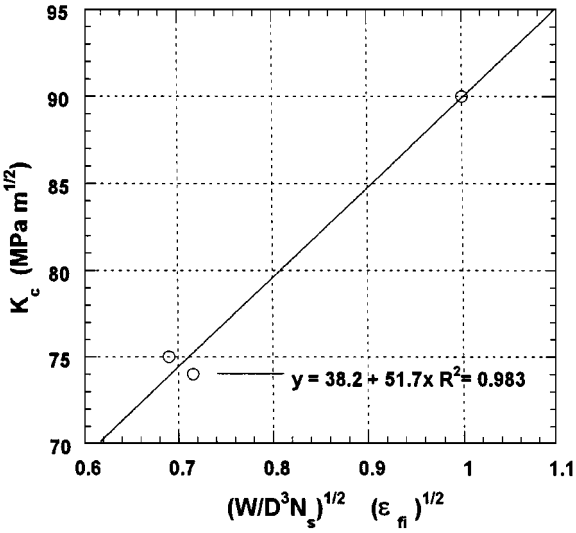

Figure 7 Experimental K_c versus $(W/D^3 N_s)^{1/2}$ for the Embury–Nes model. (——) $y = 38.2 + 51.7x$, $R^2 = 0.983$.

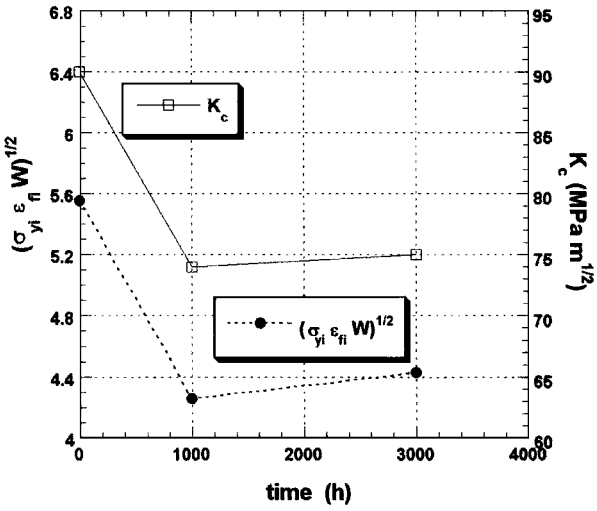

Figure 9 Experimental K_c and $(\sigma_y \varepsilon_{fi} W)^{1/2}$ versus exposure time at 135 °C. (⊟) K_c, (– – • – –) $(\sigma_{yi} \varepsilon_{fi} W)^{1/2}$.

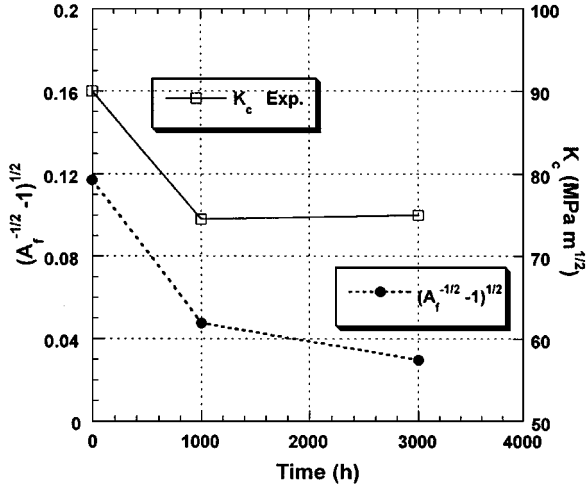

Figure 10 Experimental K_c and $(\varepsilon_{fi})^{1/2}$ versus exposure time at 135 °C. (⊟) K_c exp, (– – • – –) $(A_f^{-1/2} - 1)^{1/2}$.

(Figs 10 and 11) show a tendency for the parameter to decrease at 3000 h, with $(A_f^{-0.5} - 1)^{1/2}$ declining faster than $\varepsilon_{fi}^{1/2}$. Based on the above discussion, it appears that the Hornbogen–Graf model fits the experimental data better than does the Embury–Nes model.

The Hornbogen–Graf model also indicates that the fracture toughness is not only a function of grain-boundary parameters but also a function of matrix parameters, such as yield strength. Li and Shenoy's work indicates that the change of yield strength following thermal exposure at 1000 and 3000 h is the result of changes in the type of precipitate, number density of precipitates and their volume fraction in the matrix [4]. The slight observed recovery of fracture toughness at 3000 h for the alloy may be due to the reduction in yield strength which accompanies the longest elevated temperature exposure.

As the thermal exposure time increases, alterations in the values of microstructural parameters at the grain boundary also result in an increase in the area fraction of intergranular fracture. This has been observed by Reynolds *et al.* [2, 3]. However, a relationship between area fraction of intergranular fracture and fracture toughness is quite complicated, and is not described by a linear relationship such as that between $(\sigma_y \varepsilon_{fi} W)^{1/2}$ and K_c in Fig. 6. This may be because, in addition to changes in the amount of ductile intergranular fracture which may occur as a function of exposure time, the energy of such fracture is not a constant, i.e. not all intergranular fractures are the same.

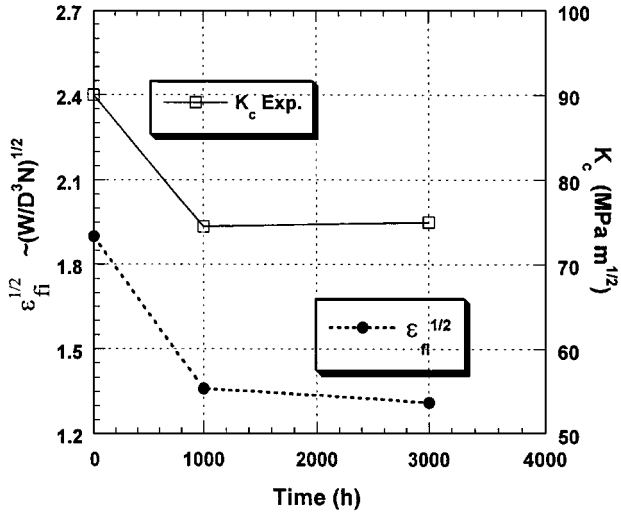

Figure 11 Experimental K_c and $(A_f^{-0.5} - 1)^{1/2}$ versus exposure time at 135 °C. (⊟) K_c exp, (– – • – –) $\varepsilon_{fi}^{1/2}$.

5. Conclusion

A simple method was developed for quantitative analysis of TEM image of grain-boundary precipitates. Grain-boundary characteristics parameters such as D, W, N_s and A_f were obtained by quantitative TEM analysis. The values of W, D and A_f increase and the value of N_s decreases after 1000 and 3000 h thermal exposure at 135 °C. These parameters were used in an equation developed by Kawabata and Izumi, to calculate the grain-boundary fracture strain, ε_{fi}. The calculated fracture strain, ε_{fi}, decreases with exposure time at 135 °C. On comparing two fracture toughness models to correlate the mechanical properties and microstructure parameters, the model developed by Hornbogen and Graf appears to show a near perfect agreement between the experimental data and calculated fracture toughness variation. It is worth noting that the model also predicts recovery of fracture toughness for the 135 °C/3000 h exposure, as borne out by the results from the present study.

Acknowledgements

The authors thank Dr A. Cho, Reynolds Metals Company, for his invaluable discussion and support. The authors thank Ms M. S. Domack, NASA Langley Research Center, for providing mechanical testing data, and Dr D. Bryant and Mr M. Bryson, Reynolds Metals Company, and Dr R. N. Shenoy, NASA Langley Research Center, for useful discussions.

References

1. J. VIETZ and I. J. POLMEAR, *J. Inst. Metals* **94** (1966) 410.
2. A. P. REYNOLDS and QIONG LI, *Scripta Mater.* **34** (1996) 1803.
3. A. P. REYNOLDS and R. E. CROOKS, in "Elevated Temperature Effects on Fatigue and Fracture," ASTM STP 1297, edited by R. S. Piascik, *et al.* (American Society for Testing and Materials, Philadelphia, PA, 1997) p. 191.
4. QIONG LI and R. N. SHENOY, *J. Mater. Sci.* (1997) in press.
5. A. K. VASUDEVAN and R. D. DOHERTY, *Acta Metall.* **35** (1987) 1193.
6. S. HALES and R. CROOKS, NASA Technical Report, May 1996 (NASA Langley Research Center, Hampton, VA, 1996).
7. I. J. POLMEAR, *Trans. Metall. Soc. AIME* **230** (1964) 1331.
8. N. SANO, K. HONO, T. SAKURAI and K. HIRANO, *Scripta Metall.* **25** (1991) 491.
9. T. KAWABATA and O. IZUMI, *Acta Metall.* **24** (1976) 817.
10. E. HORNBOGEN and M. GRAF, *ibid.* **25** (1977) 877.
11. J. D. EMBURY and E. NES, *Z. Metallk de* **65** (1974) 45.

Received 6 October 1997
and accepted 28 July 1998